AIAA SciTech Forum
6-10 January 2025, Orlando, FL
AIAA SCITECH 2025 Forum

10.2514/6.2025-2501

Investigating the Raman Characteristics of Regolith Simulants Towards the Creation of Functional Materials

M. Laura S. Johann*, Lexi J. Greenwood†, Sofia I. De Hoffmann‡, Justin Astacio§, Michael P. Kinzel¶, and Seetha Raghavan‖
Embry-Riddle Aeronautical University, Department of Aerospace Engineering, Daytona Beach, Florida, 32114

This study investigates the functionality and feasibility of materials distinguished by their regolith composition for application as sensors in extreme environments. The focus is placed on regolith composites sourced from different lunar terrains—specifically, the Lunar Highland (LH) and Lunar Mare (LM)—to assess their potential for fabricating functional and reliable sensors via digital light processing (DLP) 3D printing. Epoxy composites incorporating 10% by weight of LMS-1D and LHS-1D simulants were analyzed to determine their propensity for dispersion in a manufactured sample and the potential for leveraging their spectral emissions for sensing. The effectiveness of these materials was evaluated by measuring the Raman peaks in powder and manufactured form for peak identification as well as comparisons of the sensitivity of peakshifts and linewidth changes. These results contribute to the broader understanding of lunar regolith-based composite materials for sensor applications.

I. Nomenclature

$LMS\text{-}1D$	=	Lunar Mare Dust Simulant
$LHS\text{-}1D$	=	Lunar Highland Dust Simulant
DLP	=	Digital Light Processing
PL	=	Plagioclase
OL	=	Olivine
IL	=	Ilmenite
PX	=	Pyroxene
$FWHM$	=	Full Width at Half Maximum

II. Introduction

The increasing interest in lunar exploration and settlement necessitates an assessment of in situ resources for support of activities on the Moon. This has led to a significant increase in research efforts to manufacture structural parts from lunar and planetary regolith [1–3]. Key needs for lunar operation include monitoring and measurement of the environment and safety systems, which can be facilitated by sensors. Therefore, in-space manufacturing of functional materials that enable detection, using in situ lunar resources, is of interest [4]. Spectral emissions from Raman and photoluminescence measurements have been calibrated for a number of material systems to create stress and temperature sensors via peak dependencies [5–10]. When considering the creation of functional materials from lunar regolith, spectral peaks from the minerals within them and their potential sensitivity to environmental changes in temperature and pressure offer opportunities for sensing. This work offers a pathway for a thorough assessment of the spectral properties of lunar regolith variants, signal robustness in manufactured parts and sensitivity to external changes.

*PhD. Student Researcher, Aerospace Engineering, Embry-Riddle Aeronautical University, AIAA student member, sorgijom@my.erau.edu.
†Undergraduate Student Researcher, Aerospace Engineering, Embry-Riddle Aeronautical University.
‡Undergraduate Student Researcher, Aerospace Engineering, Embry-Riddle Aeronautical University.
§Undergraduate Student Researcher, Aerospace Engineering, Embry-Riddle Aeronautical University.
¶Associate Professor, Aerospace Engineering, Embry-Riddle Aeronautical University.
‖Professor and Associate Dean, Aerospace Engineering, Embry-Riddle Aeronautical University, AIAA Associate Fellow, seetha.raghavan@erau.edu.

A. Lunar Regolith

Regolith, the fragmented rock material that forms the land surface, occurs on Earth and the Moon. They may have initially shared chemical similarities, however, the reducing environment on the Moon results in a composition markedly distinct from terrestrial regolith. Additionally, the physical processes shaping regolith on each body differ significantly. On Earth, regolith formation is driven by terrestrial physical and chemical weathering processes, including geochemical and biochemical mechanisms. In contrast, lunar regolith forms through meteoroid impacts and exposure to cosmic radiation, which produce finer and sharper granules [11].

Lunar regolith can be classified into two primary types based on their geological origins: the elevated, feldspathic (light-colored) plains of the highland regions and the basaltic (dark-colored) plains of the lunar maria. It is these regolith sources we explore, Lunar Highland and Lunar Mare, utilizing extra fine dust simulants, LHS-1D and LMS-1D respectively [12]. The mineralogy and chemical compositions of the simulants as well as the particle size and shapes match the samples from the Apollo missions. The extra fine dust versions were chosen for manufacturing with a polymer matrix to create functional materials as they were expected to provide better adhesion, more uniform or homogeneous composites with less sedimentation.

B. Additive manufacturing of Regolith composites

Digital Light Processing (DLP) of lunar regolith is a slurry-based photopolymerization method for ceramic composites fabrication with promising capabilities in the ability to control feature resolution and surface finish while maintaining mechanical properties[13]. In considering the manufacturing of lunar regolith with this approach, the finer geometry of the simulants (mean particle size of 6 to 7 μm) was specifically selected to enhance the DLP manufacturing process, such that the increased surface area enhances adhesion with the matrix. The processing approach for the functional materials using DLP also considers the weight fraction of simulant with respect to polymer. The desired regolith weight fraction selected was 10 wt% to ensure that sufficient particle concentration is achieved for spectral peaks to be collected. At the same time, high weight fractions will increase brittleness and delamination. The electrostatic clumping behavior of the finer particles [11] must be considered when evaluating the quality of the functional materials manufactured, as this can affect performance. Dispersion characteristics are used as a key metric to achieve a homogeneous composite which is important for sensing performance. Dispersion studies in particulate composite manufacturing have been achieved using different approaches [14, 15]. The approach taken here uses high-resolution optical images to identify the particles in the manufactured material and establish a weight fraction estimation.

C. Raman Spectroscopy and Piezospectroscopic Effect

The basis for the development of functional materials such as sensors can be achieved using the spectral emissions of the materials and their dependencies on external environments. Raman spectroscopy analyzes the small fraction of laser light that is inelastically scattered by a sample, resulting in an energy shift that provides detailed information about the material's structure and bonding. The resulting spectra reveal vibrational modes, characterized by their peak positions, which correspond to the crystal lattice of the sample. For each mode, the peak intensity, position shifts, and line width at half maximum (FWHM) provide insights into the material's concentration, stress state, and crystallinity. These properties can be calibrated and exploited for sensing applications. The inherent sensing properties of regolith and regolith composites are yet to be uncovered and the first step to doing so is to investigate the various Raman spectral peaks from the rich minerals within the various regolith compositions. The complex mineral composition of both LMS and LHS lunar regolith simulants can be summarized in Table 1. Additionally, a collection of previous literature reporting known Raman peaks for each mineral type is summarized within Table 1.

The piezospectroscopic effect in composite materials has been gaining attention in non-destructive testing because of its potential for assessing stress conditions through signals generated by embedded particles. The basis of these measurements can be described, for example, when a crystal sample is subjected to uniform stress, such as hydrostatic pressure, evenly distributed strains can be quantified by measuring the unit-cell parameters of the crystal and comparing them to those of an unstrained reference crystal [21]. This principle underlies the diffraction-based methods used to determine thermal expansion and equations of state for minerals [21]. However, synchrotron X-ray diffraction (XRD) is expensive and unsuitable for the routine analysis of numerous grains or inclusions, but Raman spectroscopy offers a practical alternative [21]. Raman shifts in inclusions are typically interpreted as the result of hydrostatic pressure within the inclusion. These shifts are converted into pressure values using established pressure-wavenumber calibration curves [21].

Table 1 Mineral composition of LHS and LMS regolith simulant used within this study as well as the known Raman peaks of the minerals within the lunar simulants

Mineral	LHS wt%	LMS wt%	Known Raman Peaks (cm^{-1})
Pyroxene	0.3	32.8	
(Ortho)			331-338,388,657,673-679,1001-1007 [16–18]
(Clino)			317,339,653,663-665,995,1005 [16, 18, 19]
Glass-rich Basalt	24.7	32	757,970 [19]
Anorthosite	74.4	19.8	483-488,503-505,557-564 [16, 18, 20]
Olivine	0.2	11.1	815-826,847-856 [16, 18, 19]
Ilmenite	0.4	4.3	681 [19]

Although the potential parameter-sensitive peaks and their dependencies that would yield absolute values of piezospectroscopic coefficients are unknown for our material of interest, preventing direct measurement of strain, stress, or other parameters, this study explores the material's responsiveness to the manufacturing process as an indirect approach. Specifically, we investigate the spectral changes in regolith samples, analyzing their transition from raw powders to manufactured states. This preliminary analysis identifies promising Raman peaks that could serve as reliable indicators for stress-sensing applications.

III. Experimental and Analysis Methods

The samples were manufactured using both LMS-1D and LHS-1D powders. The manufacturing process for samples using DLP is described in our published work [4] and summarized here. Both resin and regolith were added together and thoroughly mixed under a fume hood using a THINKY mixer AR-100 ensuring particle dispersion. This was followed by defoaming to mitigate entrapped microbubbles within the matrix. The samples were then printed using a DLP printer with a 5μm layer thickness and cured with 405 nm UV light for 6 seconds per layer. Post-processing included an isopropyl alcohol wash and additional UV curing for 3 minutes on each side of the sample. A typical sample produced by this approach is shown in Fig 1.a. Optical images of the surfaces of both the LMS-1D and LHS-1D samples were taken as shown in Fig 1.b to conduct a dispersion analysis. Raman spectroscopy data was collected with a WITec Alpha 300RA Confocal Raman microscope equipped with a He:Ne 532 nm laser excitation source as shown in Fig 1.c.

A. Dispersion Analysis Methodology

The particle distribution was quantified by analyzing 500x microscope images of each section. To enhance particle visibility, image contrast, saturation, and brightness were adjusted to better expose particle features. Each particle was then measured using the freehand tool in ImageJ software. The major and minor axes of the particles were recorded to calculate the mean particle size in pixel length, which was subsequently converted to micrometers. The particle size distribution was evaluated using the Krumbein phi scale (ϕ) to categorize particle types (e.g., silt, clay, colloid) and assess their dispersion during the DLP printing process.

$$\phi = -log_2 \frac{D}{D_0} \tag{1}$$

Where D represents the diameter of the particle in millimeters and D_0 is a reference diameter set to 1 mm to ensure dimensional consistency within the equation.

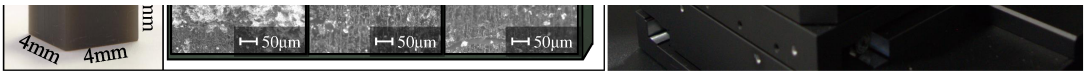

Fig. 1 a) An optical image of a DLP 3D printed LMS-1D sample, b) 500x magnification optical microscope images of the LMS and LHS DLP samples, c) the Raman spectroscopy system used, and d) the resulting and processed spectra produced from a Raman measurement.

B. Raman Analysis Methodology

The Raman measurements were performed with a commercial confocal and continuous wave (cw) Raman microscope laser (WITec alpha300 R system) with an excitation wavelength of 532 nm. The laser was focused to a spot of approximately 0.720 μm, using a 100x magnification objective with a numerical aperture of 0.9. Thus, the beam spot size was smaller than the mean particle size of the regolith inclusions. The spectral resolution of 1 cm^{-1} was achieved with a groove density of 1800 g/mm. An image of the Raman setup is shown in Fig. 1 a).

A minimum of 10 points were measured within a 200 x 200 μm sampling area, with an integration time of 2 seconds per point, accumulated 20 times. As shown in Fig. 1 b), Raman measurements were conducted on a series of LMS and LHS DLP-printed regions. To process the data, an algorithm was scripted in Python for baseline correction using asymmetric least squares smoothing, followed by final profile smoothing with a Gaussian window spanning two observation points. Pseudo-Voigt profiles were used to deconvolute and fit peaks of interest, allowing investigation into how the manufacturing process affects peak shifts, line width changes, and the material's potential for sensor applications.

IV. Results and Discussion

A. Dispersion analysis

Fig 2.a and 2.b show the particle size dispersion of the LHS-1D samples along with the analysis using ImageJ and the final distribution of the particle sizes for the samples. Similarly, Fig 2.c and 2.d show these results for the LMS-1D sample. For both LMS and LHS samples, there is a good overall distribution of particle sizes that is representative of the simulant specifications [12]. Consequently, the variation in the distribution of particles in the different sections of the sample can be attributed to the DLP process. The results show that the left sides of each sample have a distribution of larger particle sizes, while the middle has finer particles followed by a mix of sizes for the right side. This could be interpreted as the left side representing the first layers in a typical DLP printing process where the slurry has a good mix of particle sizes with large particles dominating since they have not yet settled. Over time, when the layers of the middle section are printed, large particles have settled and only fine dust are deposited, resulting in small particle size distribution. As the last few layers are printed (making the right section), the remaining slurry is filled with some of the larger settled particles, and so the particle size distribution skews right once again.

Fig. 2 a) LHS-1D particle size dispersion analysis and b) LHS-1D particle size dispersion analysis, c) LMS-1D particle size dispersion analysis and d) LMS-1D particle size dispersion analysis.

B. Raman characterization

An average of the Raman spectra captured for LHS is shown in Fig. 3a for the manufactured DLP sample, top spectra, and the LHS powder sample, bottom spectra. Similarly, Fig. 3b shows the Raman spectra captured for LMS with the top spectra coming from the LMS powder and the bottom spectra from the manufactured DLP sample.

Peak identification was performed using the peaks listed Table 1 above. From these spectra, anorthosite (plagioclase PL), pyroxene (PX), olivine (OL), and ilmenite (IL) were found to have a strong Raman response. Shifts in the peak locations can be easily observed from the powder to DLP spectra. Similarly, a separation of the peaks can also be observed for prominent peaks when comparing the spectra of the powder and DLP samples. This separation of the peaks is more easily observed in doublets such as the anorthosite peaks around 485 cm^{-1} and 505 cm^{-1} as well as the olivine peaks around 820 cm^{-1} and 850 cm^{-1}.

The olivine doublet at around 820 cm^{-1} and 850 cm^{-1} is of keen interest due to its strong Raman response and relative isolation from surrounding Raman peaks in both LHS and LMS. A pseudo-Voigt deconvolution and subsequent peak fitting were used on the 820 and 850 cm^{-1} doublet peaks of olivine, which are shown in Fig. 4. Fig. 4a are the pseudo-Voigt fitting results for the LHS DLP and LHS powder olivine doublet peaks and Fig. 4b are the results for the LMS DLP and LMS powder olivine doublet peaks.

The peak center positions relative to the Raman shift, cm^{-1}, as well as the FWHMs of the peaks labeled within Fig. 4. Changes in signal intensities can most likely be attributed to differences in regolith simulant particle sizes and concentrations. The powder form of these simulants has a much higher particle density than the samples manufactured 10% with DLP. This effectively increases the likelihood of the laser probing and exciting the regolith simulant, relative to their compositional wt% distribution of minerals. DLP samples were also probed mostly through resin, which has a relatively poorer Raman response compared to the oxides comprising the regolith simulants. This would result in a reduced Raman spectra signal. It should be noted that LHS also has a much lower concentration of olivine as compared to LMS, which will decrease the potential intensity of the spectra and the likelihood of encountering olivine with small laser spot sizes.

Fig. 5a plots the changes in the peak center position and Fig. 5b plots the changes in the FWHM for the LHS

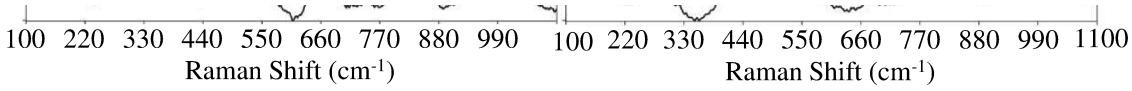

Fig. 3 a) Raman spectra and peak identification of the LHS powder and LHS DLP samples and b) of the LMS powderand LMS DLP samples. Peaks were identified using Table 1 and their respective associated minerals are labeled for each peak identified in the spectra.

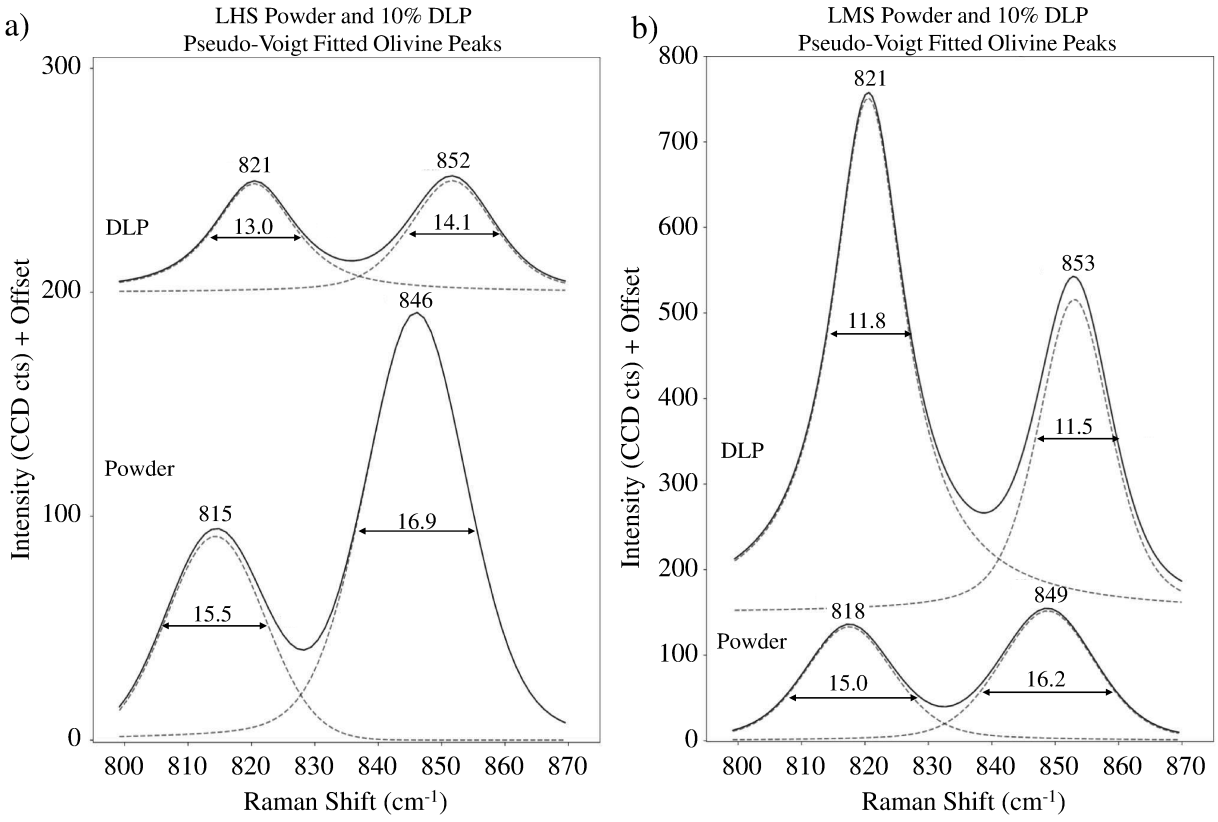

Fig. 4 Pseudo-Voigt deconvolution results of the Olivine doublet peaks, 820 cm^{-1} and 850 cm^{-1} for the a) LHS regolith and b) LMS regolith, where the top spectra represents the manufactured DLP sample and the bottom spectra represents the powder of these simulants. The peak center positions and FWHMs for each peak are labeled on in the plots.

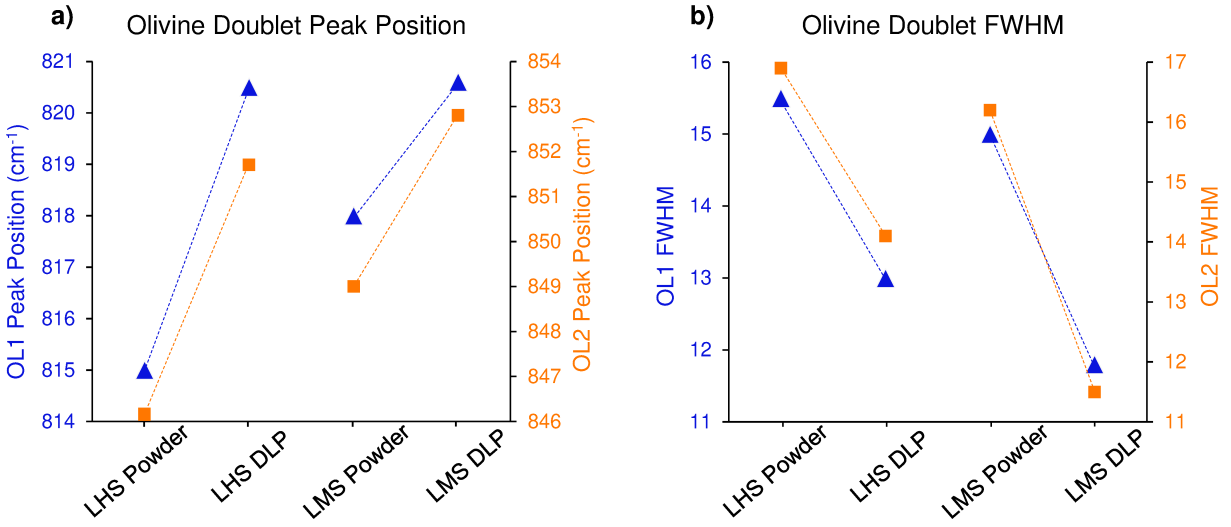

Fig. 5 Summary of the a) peak center positions and b) FWHMs of the Olivine doublet peaks, 820 cm^{-1} (OL1) and 850 cm^{-1} (OL2) for the LHS powder, LHS DLP, LMS powder, and LMS DLP samples.

Powder, LHS DLP, LMS Powder, and LMS DLP samples. The 820 cm^{-1} olivine peak is tracked by the blue triangle (OL1) while the 850 cm^{-1} olivine peak is tracked by the orange square (OL2). In general, a blue shift, a rightward shift to a higher wavenumber, is observed for both olivine peaks in the peak center locations from its powder form to the manufactured DLP sample. These blue shifts are likely due to the DLP manufacturing process itself. This is because the DLP samples are of their respective regolith simulants embedded within a UV-curable resin. The blue shift for both simulant DLP samples suggests there is likely some residual stress induced onto the particles from the surrounding resin matrix, likely as a result of the shrinking and cooling of the resin during curing. Additional work is required to determine if this blue shift is the result of the regolith particles being pulled by the surrounding resin matrix, resulting in the regolith experiencing tensile residual stresses, or is the result of the particles being compressed by the surrounding resin matrix, resulting in the regolith experiencing compressive residual stresses.

Additional tests, using the simulant powder form as a stress reference, can be performed to quantify the amount of residual stress the DLP manufactured samples experience as a result of the manufacturing process. The relationship between applied stress from a hydrostatic force and the shifting of the peak center positions can then be used to obtain and quantify the piezospectropic coefficient. Finding the piezospectropic coefficient, the slope between applied stress and peak shift, will give insight on the 820 cm^{-1} and 850 cm^{-1} olivine doublet's sensitivity to stress changes. A high sensitivity is vital for a high resolution regolith sensor measuring applied external stresses and temperature changes. Further exploration of other Raman responsive minerals within the simulants, such as anorthosite, can be performed to observe their sensitivities and effectiveness to changing environmental conditions similar to conditions experienced in the extreme lunar environment.

Fig. 4 and Fig. 5 also show the FWHM of both olivine peaks narrowing when comparing the powder spectra with the DLP manufactured spectra. This reduction in the FWHM is likely due to the decrease in the number of regolith simulant particles being probed, reducing the number of different orientations and bindings of the molecules being measured within the probed laser region. However, it should be noted the number of different orientations of the particles may also be reduced as a result of the DLP manufacturing method. DLP being a form of 3D printing, there are directional layering created during the manufacturing process. This directional orientation will introduce anisotropic properties to the sample, resulting in a preferred orientation in the composite. This more preferred orientation of the molecules from the olivine would result in more sharp peaks, lowering FWHM. Alternatively, the decrease in FWHM may be attributed to the higher heat tolerance of the composite material, in contrast to the powder form, which is more prone to heat-induced deformation.

Additional work can observe how DLP manufacturing influences the orientation of the regolith simulants. A comparison with a non-inherently anisotropic manufacturing process of 10% weight LHS and LMS samples with the DLP samples would provide insights on the spectral response properties, such as FWHM, of the regolith in embedded matrix composite systems and for sensor-based applications. A more narrow FWHM, as a result of preferred orientations, would provide a sharper and more sensitive response toward external forces and conditions acting on that preferred direction while compromising on the sensor's response and reducing its sensitivity transverse to the preferred direction. In other words, the sensor would perform better in the preferred direction, with higher sensitivity, compared to any other direction, which may be ideal in specialized cases, such as uniaxial load monitoring. Conversely, a more broad FWHM, as a result of no preferred orientation, would provide a balanced response from the sensor towards external forces with a uniform sensitivity in any direction. In other words, the sensor would likely perform, overall, more balanced in any direction at a lower overall sensitivity, which might be ideal in more general applications for non-uniaxial external loading.

V. Conclusion

This study investigated the functionality and feasibility of regolith for sensor-based development in extreme environments. Regolith simulants used were comprised of minerals sourced from the lunar highland and lunar mare regions, LHS and LMS respectively. These simulants were embedded at 10 wt.% into a resin through digital light processing (DLP) 3D printing. A dispersion study as well as Raman spectroscopy were utilized to determine the feasibility and functionality of using lunar regolith as reliable sensors. A comparison was made between the simulants in their powder forms as well as DLP 3D printed forms. The dispersion of particles, by size, was done throughout the DLP 3D printed sample. The Raman spectral peaks of the minerals were identified. An olivine doublet at 820 cm^{-1} and 850 cm^{-1} was selected as a potential marker for sensing capabilities due to its strong Raman response and relative isolation from other Raman signals. The shifts between the peak center positions and narrowing of the FWHM of the peaks were observed from the powder regolith to the DLP samples. These results serve as an initial baseline towards a

further and a much broader understanding of the capabilities of lunar regolith-based composites to be used for lunar sensor-based applications.

Acknowledgments

This material is based upon work supported by National Science Foundation grant CMMI 2349931. Additionally, the authors would like to acknowledged ERAU PhD student, Zachary Stein, for his valuable support.

References

[1] Warren, P., Raju, N., Ebrahimi, H., Krsmanovic, M., Raghavan, S., Kapat, J., and Ghosh, R., "Effect of sintering temperature on microstructure and mechanical properties of molded Martian and Lunar regolith," *Ceramics International*, Vol. 48, No. 23, 2022, pp. 35825–35833.

[2] Torre, R., Cowley, A., and Ferro, C. G., "Low binder content bricks: a regolith-based solution for sustainable surface construction on the Moon," *Discover Applied Sciences*, Vol. 6, No. 3, 2024, p. 88.

[3] Mariani, M., Bertolini, F., Isachenkov, M., Galassi, C., Lecis, N., Grande, A., Sala, G., et al., "Binder Jetting of Lunar Regolith: 3D Printing and Densification," *75th International Astronautical Congress (IAC 2024)*, 2024, pp. 1–8.

[4] Astacio, J., Johann, M. L. S., Stein, Z., Facchini, L., Wischek, J., Bartsch, M., Kinzel, M., and Raghavan, S., "In-space manufacturing of functional sensors," *International Astronautical Congress*, IAF Microgravity Sciences and Processes Symposium (A2), Vol. 75, International Astronautical Federation (IAF), Milan, Italy, 2024.

[5] Stevenson, A., Jones, A., and Raghavan, S., "Stress-Sensing Nanomaterial Calibrated with Photostimulated Luminescence Emission," *Nano letters*, Vol. 11, No. 8, 2011, pp. 3274–3278.

[6] Stevenson, A., Jones, A., and Raghavan, S., "Real-time monitoring of an adhesive lap shear test using piezospectroscopy," *52nd AIAA/ASME/ASCE/AHS/ASC Structures, Structural Dynamics and Materials Conference 19th AIAA/ASME/AHS Adaptive Structures Conference 13t*, 2011, p. 1814.

[7] Freihofer, G., Fugon-Dessources, D., Ergin, E., Van Newkirk, A., Gupta, A., Seal, S., Schu?lzgen, A., and Raghavan, S., "Piezospectroscopic measurements capturing the evolution of plasma spray-coating stresses with substrate loads," *ACS applied materials & interfaces*, Vol. 6, No. 3, 2014, pp. 1366–1369.

[8] Freihofer, G., Schülzgen, A., and Raghavan, S., "Damage mapping with a degrading elastic modulus using piezospectroscopic coatings," *NDT & E International*, Vol. 75, 2015, pp. 65–71.

[9] Fouliard, Q., Ghosh, R., and Raghavan, S., "Quantifying thermal barrier coating delamination through luminescence modeling," *Surface and Coatings Technology*, 2020, p. 126153.

[10] Freihofer, G., Schülzgen, A., and Raghavan, S., "Multiscale mechanics to determine nanocomposite elastic properties with piezospectroscopy," *Acta Materialia*, Vol. 81, 2014, pp. 211–218.

[11] Long-Fox, J., and Britt, D., "Characterization of planetary regolith simulants for the research and development of space resource technologies," *Frontiers in Space Technologies*, Vol. 4, 2023. https://doi.org/10.3389/frspt.2023.1255535.

[12] Madison, A., Landsman, Z., Long-Fox, J., Metke, A., Krol, K., Easter, P., C.Sipe, and L. Weber, D. B., "Lunar Dust Simulants and Their Applications," *Proceedings of Earth and Space*, 2022.

[13] Chen, Z., Li, Z., Li, J., Liu, C., Lao, C., Fu, Y., Liu, C., Li, Y., Wang, P., and He, Y., "3D printing of ceramics: A review," *Journal of the European Ceramic Society*, Vol. 39, 2019, p. 661–687.

[14] Hanhan, I., Selimov, A., Carolan, D., Taylor, A. C., and Raghavan, S., "Quantifying alumina nanoparticle dispersion in hybrid carbon fiber composites using photoluminescent spectroscopy," *Applied Spectroscopy*, Vol. 71, No. 2, 2017, pp. 258–266.

[15] Stevenson, A., Jones, A., and Raghavan, S., "Stress-Sensing Nanomaterial Calibrated with Photostimulated Luminescence Emission," *Nano Letters*, Vol. 11, No. 8, 2011, pp. 3274–3278. https://doi.org/10.1021/nl201626q, pMID: 21707042.

[16] Ling, Z., Wang, A., and Jolliff, B. L., "Mineralogy and geochemistry of four lunar soils by laser-Raman study," *Icarus*, Vol. 211, No. 1, 2011, pp. 101–113. https://doi.org/https://doi.org/10.1016/j.icarus.2010.08.020.

[17] Zhao, S., and Wallaschek, J., "A standing wave acoustic levitation system for large planar objects," *Archive of Applied Mechanics*, Vol. 81, 2011, pp. 123–139. https://doi.org/10.1007/s00419-009-0401-3.

[18] Wang, A., Jolliff, B. L., and Haskin, L. A., "Raman spectroscopy as a method for mineral identification on lunar robotic exploration missions," *Journal of Geophysical Research: Planets*, Vol. 100, No. E10, 1995, pp. 21189–21199. https://doi.org/https://doi.org/10.1029/95JE02133.

[19] Zhao, H., Meng, L., Li, S., Zhu, J., Yuan, S., and Zhang, W., "Development of lunar regolith composite and structure via laser-assisted sintering," *Frontiers of Mechanical Engineering*, Vol. 17, 2022. https://doi.org/10.1007/s11465-021-0662-2.

[20] Freeman, J., Wang, A., Kuebler, K., Jolliff, B., and Haskin, L., "Characterization of natural feldspars by Raman spectroscopy for future planetary exploration," *The Canadian Mineralogist*, Vol. 46, 2008, pp. 1477–1500. https://doi.org/10.3749/canmin.46.6.1477.

[21] Angel, R. J., Murri, M., Mihailova, B., and Alvaro, M., "Stress, strain and Raman shifts," *Zeitschrift für Kristallographie - Crystalline Materials*, Vol. 234, No. 2, 2019, pp. 129–140. https://doi.org/doi:10.1515/zkri-2018-2112.